RESEARCH ARTICLE

American Society of Plant Biologists   S·E·B SOCIETY FOR EXPERIMENTAL BIOLOGY   WILEY

A K homology (KH) domain protein identified by a forward genetic screen affects bundle sheath anatomy in *Arabidopsis thaliana*

Zahida Bano [ORCID] | Peter Westhoff [ORCID]

Institute of Plant Molecular and Developmental Biology, Heinrich-Heine-University, Düsseldorf, Germany

Correspondence
Peter Westhoff, Institute of Plant Molecular and Developmental Biology, Universitätsstrasse 1, Heinrich-Heine-University, 40225 Düsseldorf, Germany.
Email: west@uni-duesseldorf.de

Abstract

Because of their photosynthetic capacity, leaves function as solar panels providing the basis for the growth of the entire plant. Although the molecular mechanisms of leaf development have been well studied in model dicot and monocot species, a lot of information is still needed about the interplay of the genes that regulate cell division and differentiation and thereby affect the photosynthetic performance of the leaf. We were specifically interested in understanding the differentiation of mesophyll and bundle sheath cells in *Arabidopsis thaliana* and aimed to identify genes that are involved in determining bundle sheath anatomy. To this end, we established a forward genetic screen by using ethyl methanesulfonate (EMS) for mutagenizing a reporter line expressing a chloroplast-targeted green fluorescent protein (sGFP) under the control of a bundle sheath-specific promoter. Based on the GFP fluorescence phenotype, numerous mutants were produced, and by pursuing a mapping-by-sequencing approach, the genomic segments containing mutated candidate genes were identified. One of the lines with an enhanced GFP fluorescence phenotype (named *ELEVATED BUNDLE SHEATH CELLS SIGNAL 1 [ebss1]*) was selected for further study, and the responsible gene was verified by CRISPR/Cas9-based mutagenesis of candidate genes located in the mapped genomic segment. The verified gene, At2g25970, encodes a K homology (KH) domain-containing protein.

KEYWORDS
Arabidopsis thaliana, bundle sheath cells, CRISPR/Cas9, ethyl methanesulfonate, green fluorescent protein, KH domain

1 | INTRODUCTION

Leaves are the organs of photosynthesis, capturing light energy and converting it into chemical energy via the photosynthetic machinery located in the chloroplasts of its chlorenchyma cells. The development of a leaf is complex and relies on the precise regulation of various steps such as cell division, proliferation, and cell differentiation. These developmental processes have been extensively studied in the model plants *Arabidopsis thaliana* and *Zea mays*, and numerous regulators of leaf development could be identified with various genetic approaches (Conklin et al., 2019; Nakayama et al., 2022; Nelissen et al., 2016; Nikolov et al., 2019), but it is still poorly understood with respect to

how anatomy and morphology of a leaf influence its photosynthetic performance. Such an information, however, is required, if the photosynthetic output of a leaf (Long et al., 2015; Ort et al., 2015) is to be enhanced or if its mode of photosynthesis is to be redesigned by introducing a C_4-like photosynthetic pathway into C_3 crops (Ermakova et al., 2020; Mitchell & Sheehy, 2006).

The high efficiency of C_4 photosynthesis is intimately associated with a division of labor between two different leaf cell types, mesophyll and bundle sheath cells (Hatch, 1987), that are organized in a wreath-like structure called Kranz anatomy (Dengler & Nelson, 1999; Sedelnikova et al., 2018). Promoter reporter gene studies have shown that bundle sheath specific/preferential promoters of the genes encoding the P and the T subunits of glycine decarboxylase the Asteracean C_4 species *Flaveria trinervia* maintain the BS expression in the Brassicacean C_3 species *A. thaliana* (Emmerling, 2018; Engelmann et al., 2008; Wiludda et al., 2012). Vice versa, the bundle sheath specific/preferential promoter of the sulfate transporter gene *SULTR2;2* of *A. thaliana* was shown to retain BS specificity in the C_4 species

Flaveria bidentis (Kirschner et al., 2018). These findings suggested that the gene regulatory systems of the bundle sheath in these two families share a large degree of conservation, although the two families separated about 125 Mya years ago (Westhoff & Gowik, 2010). Because of its easy genetic tractability, *A. thaliana* should therefore be a straightforward genetic system to identify genes affecting the development and function of the bundle sheath in dicots (Döring et al., 2019; Westhoff & Gowik, 2010).

Since alterations in the size of bundle sheath cells or their chloroplast numbers are difficult to detect in large-scale phenotypic screens, we pursued a reporter gene strategy (Page & Grossniklaus, 2002). The bundle sheath and its chloroplasts were labeled by a chloroplast-targeted green fluorescent protein (sGFP; Figure 1a; Döring et al., 2019) that was driven by the bundle sheath preferential *GLDPA* promoter of *F. trinervia* (Engelmann et al., 2008). We expected that an increase in bundle size/volume or in chloroplast numbers due to a mutation should lead to an enhanced GFP fluorescence. Seeds from homozygous lines of *A. thaliana* carrying the p$GLDPA_{Ft}$::TP$_{RbcS}$-sGFP
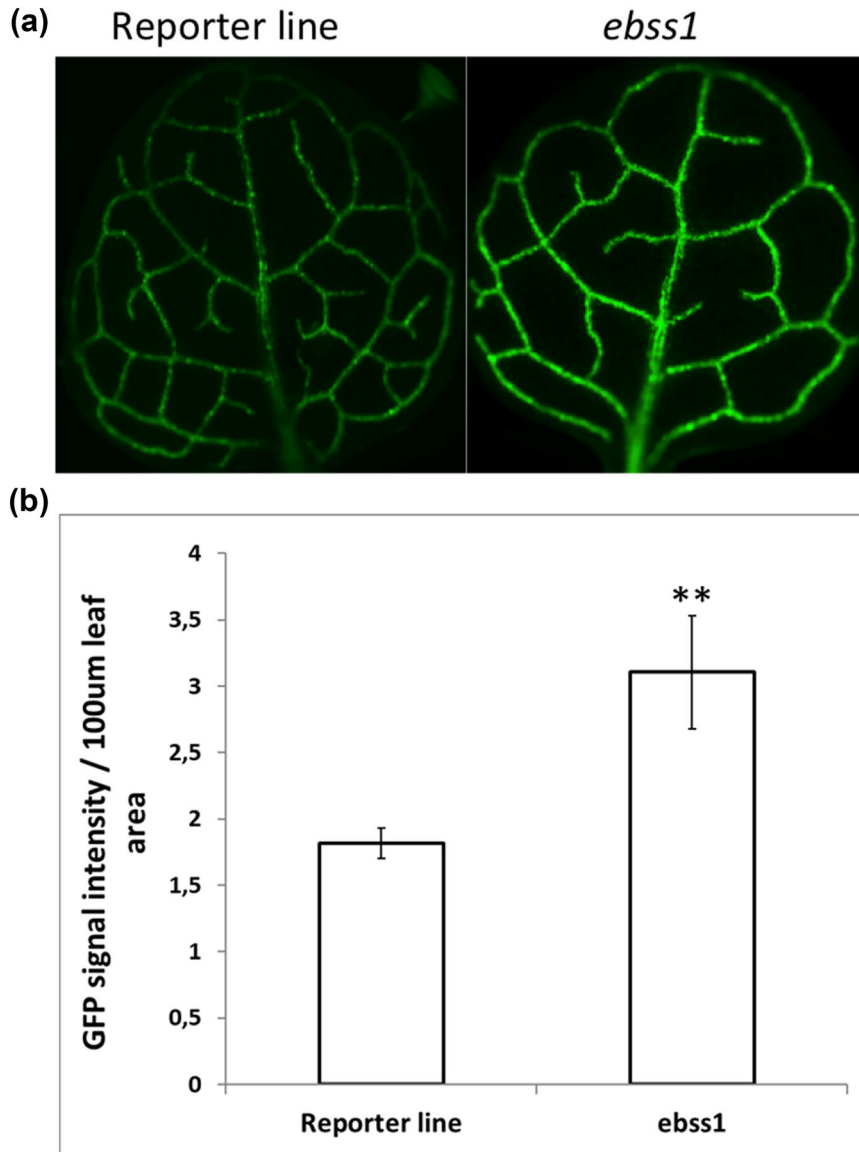

(a) Reporter line   *ebss1*

(b)

FIGURE 1 Fluorescent characteristics of *ebss1* compared with the reporter line. (a) GFP fluorescence images of the first leaf of 3-week-old EMS lines *ebss1* and the reporter line. (b) Relative changes of the GFP signal intensity in *ebss1*, the reporter line. The relative signal intensity was measured from the whole leaves of 15 plants and normalized with the leaf area. The data show mean ± SD from 15 individuals, the asterisk (**) indicates a *t*-test $P < .01$.

reporter gene construct (called the reporter line) were mutagenized with ethyl methansulfonate (EMS), and stable mutant lines of the M2 generation showing aberrant GFP expression were chosen for further analysis. Mutant loci were located by applying the SHORE mapping approach (Schneeberger et al., 2009) to a F2 backcross population constructed by crossing homozygous mutant F2 plants to the non-mutagenized reporter line (Döring et al., 2019).

In this study, we selected the *ELEVATED BUNDLE SHEATH CELLS SIGNAL 1 (ebss1)* mutant line (Figure 1a) for identifying the causative candidates for the *ebss1* mutant phenotypes. The candidate genes that were located in the mapping interval were tested for being responsible for the mutant phenotype by using CRISPR/Cas9 genetic modification (Schiml et al., 2014). By this approach, we identified At2g25970 encoding a K homology (KH) domain-containing protein to be responsible for the *ebss1* mutant phenotype.

2 | MATERIALS AND METHODS

2.1 | Mutant screening, mapping of mutant loci, and growth of plants

The mutagenesis of the p$GLDPA_{Ft}$::TP$_{RbcS}$-sGFP reporter line of *A. thaliana* (ecotype Columbia) with EMS, the screening and isolation of candidate mutants, the SHORE mapping of mutant loci, and conditions for growing Arabidopsis plants have been described by Döring et al. (2019).

2.2 | Preparation of CRISPR/Cas9 constructs

For CRISPR/Cas9 constructs, 20-bp-long single guide RNAs (sgRNAs) were designed from the gene of interest (GOI) containing PAM motif (NGG) sequences. The sgRNAs were designed in such a way that they targeted an exon of GOI and preferably no off-target sequence with maximum mismatches number 3 (http://www.rgenome.net/cas-offinder/). Primers (Table S1; 1/2 for At2g24610, 7/8 for At2g25220, 14/15 and 17/18 for At2g25970) were annealed, and the annealed primers were ligated (50-ng PFH6, 1-μL T_4 ligase, 2-μL T_4 buffer, 1.16-ng sgRNA, and H_2O up to 20 μL) into *Bbs1*-digested plasmid PFH6 (GenBank accession number KY080689; Hahn et al., 2017). After transformation into DH5α competent *E. coli* cells (ThermoFisher Scientific), colonies of recombinant bacteria were selected, and the correct insertion of the guide RNA was confirmed by Sanger sequencing (LGC Genomics, Berlin, Germany). sgRNA including the entire U6-26 promoter-sgRNA cassette was amplified from PFH6 using Phusion PCR polymerase (Table S1; 36/38 and 37/39), and after purification on agarose gels, the sgRNA was cloned into *KpnI/HindIII*-digested vector pUB-Cas9 (GenBank accession number KY080691; Hahn et al., 2017) through Gibson cloning (Gibson et al., 2009). Recombinant colonies were identified by PCR, and plasmid DNA was isolated from positive colonies by using the Qiagen MiniPrep Kit and verified by sequencing (Hahn et al., 2017).

2.3 | Transformation of *A. thaliana* with CRISPR/Cas9 constructs and selection of positive transformants

The CRISPR/Cas9 constructs carrying the sgRNA of the At2g24610, At2g25220, and At2g25970 genes in vector pUB-Cas9 were transformed into *Agrobacterium tumefaciens* strain AGL1 by electroporation (Lazo et al., 1991). Positively transformed Agrobacterium cells were verified by colony PCR followed by digestion of the extracted plasmids by suitable restriction enzyme and transformed into the reporter line via the floral dipping method (Zhang et al., 2006).

Surface-sterilized seeds of the CRISPR/Cas9-mutated reporter plants were sown on Petri dishes containing half-strength Murashige and Skoog medium containing 50-μg mL^{-1} hygromycin B (H0654, Sigma Aldrich), and hygromycin resistant plants were finally transferred to soil as describe in Döring et al. (2019). Whole-genomic DNA was isolated from 5-week-old T1 plants mutated in At2g24610, At2g25220, and At2g25970, and the presence/absence of Cas9 was assessed with PCR amplification (Table S1; 36/37). All T1 plants were self-pollinated and screened in the T2 and T3 generations to get homozygous mutant lines. The mutant screening was initially based on GFP signal followed by PCR amplification of the mutated gene and confirmation by Sanger sequencing.

2.4 | Mutant screening in the T2 generation and quantification of GFP signal

The first rosette leaf pairs of 17-day-old T2 plants of At2g24610, At2g25220, and At2g25970 were screened for aberrant GFP expression under a fluorescent binocular microscope (Axio Imager M2m Zeiss, Oberkochen, Germany). After that, leaf genomic DNA was isolated from T2 plants (10 plants for each line) and amplified with gene-specific primers (Table S1; 3/4, 10/11, and 18/19) using Phusion High Fidelity DNA polymerase. PCR products were purified using the Qiagen PCR Purification Kit and then sequenced to detect Cas9-induced mutations. Selected homozygous mutant lines were screened again in T3 and T4 generations to confirm the aberrant GFP phenotype compared with the *ebss1* and reporter line. The GFP signal intensity was measured from whole leaves using Image J and normalized to the leaf area (Döring et al., 2019; Schneider et al., 2012).

2.5 | Microscopic analysis of leaf tissue

Leaf tissue was prepared for light microscopy according to Akhani and Khoshravesh (2013). Fully expanded second leaves of 25-day-old plants were used, which were grown under optimal light conditions (16 h light and 8 h dark, by 22°C). Leaf edges and the midvein were removed, and the remaining of the leaf was cut horizontally to use the mid area (3 × 5 mm) of the leaf. Leaf samples were

immediately fixed in the solution containing 1% glutaraldehyde, 1 paraformaldehyde, and .1 M sodium cacodylate. The fixed leaf tissues were washed twice with sodium cacodylate (30-min incubation each) followed by post-fixation in 1.5% osmium tetraoxide (OsO4) for 3 h. Leaf samples were then rinsed twice (each 30 min) with a fixative solution followed by dehydration in a gradient of ethanol starting from 10% and ending at 100% (1-h incubation in each step). Tissues were then infiltrated and embedded subsequently in Araldite resin:propylene oxide solutions (1:3, 1:1, 3:1, and 100% Araldite) followed by final polymerization for 72 h at 60°C. The resin-embedded blocks were then cut with a microtome to obtain 2-μm-thick sections and stained with toluidine blue.

2.6 | RNA quantification by quantitative real-time PCR (qPCR)

Total RNA was isolated using RNeasy Plant Mini Kit (Qiagen) from rosette leaf of 25-day-old plants grown under standard growth conditions. cDNA was synthesized from 1-ug RNA using the Quantitect Reverse Transcription Kit (Qiagen, Hilden, Germany), and the purity and integrity of the cDNA were verified by agarose gel electrophoresis. qPCR was performed with KAPA SYBR FAST qPCR Master Mix Universal (KAPA Biosystem, Roche Sequencing and Life Science) using the ABI7500 Fast Real-Time PCR system following the standard procedure. The gene-specific primers used in the qPCR amplified 120- to 150-bp coding region of the gene (Table S1; 22/23, 24/25, 26/27, and 28/29). The abundance of actin primers was used as a reference (Table S1; 30/31).

2.7 | Leaf size measurement

The second rosette leaf pairs of 24-day-old mutant lines *ebss1*, *At2g25970-1*, *At2g25970-2*, *At2g25970-3*, and reporter line were photographed and measured the leaf area with image J (Version 2..0-rc-69/1.52p).

3 | RESULTS

The EMS mutant line *ebss1* was isolated from the forward genetic screening of *A. thaliana* as explained in Döring et al. (2019). The *ebss1* mutant line showed an elevated level of signal intensity of the *GFP* reporter gene in bundle sheath and vascular tissue (Figure 1a). Quantification of GFP signal intensity showed more than a 30% increase in the expression of the reporter gene (Figure 1b).

3.1 | Location and effects of the mutations in the candidate genes At2g24610, At2g25220, and At2g25970

Applying an allele frequency > .9 in SHOREmapping (see Figure S1) revealed three candidate genes for the *ebss1* mutant line (At2g24610, At2g25220, and At2g25970) that were located on chromosome II in a sequence interval between 10 and 12 Mbp (Figure 2). In each of the candidate genes, the EMS-induced mutations resulted in a single nucleotide polymorphism (SNP) within the coding region. In At2g24610, the SNP was located in exon-3, changing the 716th codon
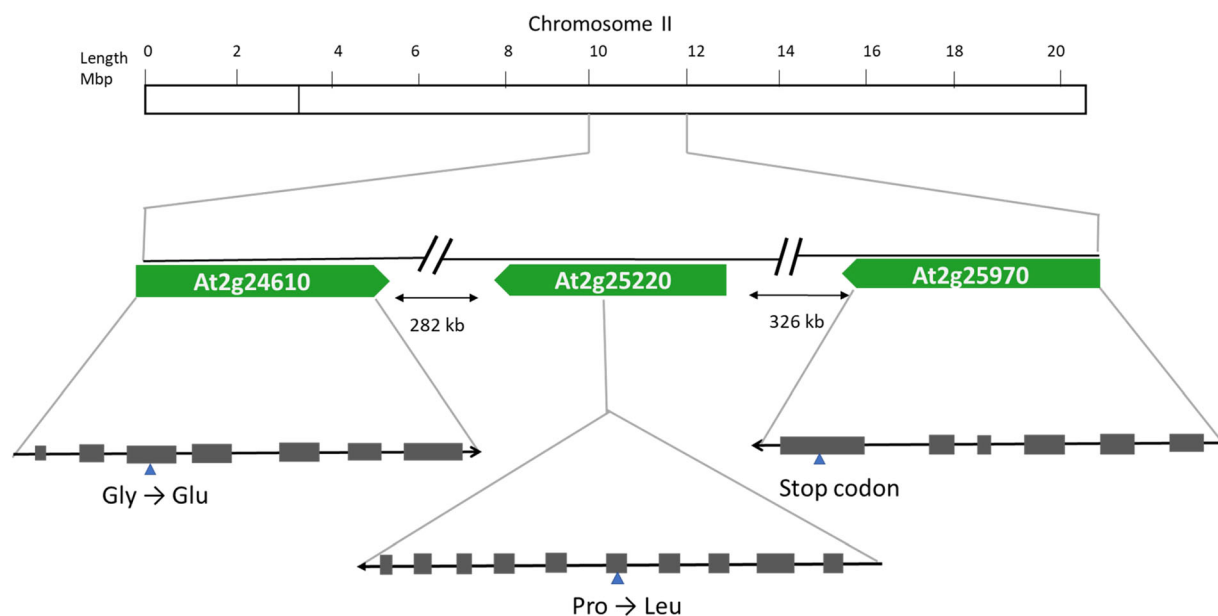

FIGURE 2 Mapping and location of candidate genes of the *ebss1* mutation on chromosome II. Allelic frequencies for all SNP were isolated from whole-genomic sequencing of the reporter line and backcrossed F2 mutants as described (Döring et al., 2019). Genes showing allelic frequencies > .9 were selected as candidate genes. The blue triangle denotes the SNP positions.

from GGA to GAA and resulting in an amino acid substitution of Glycine to Glutamic acid. In At2g25220, the mutation was observed in exon-5, altering the 716th codon from CCT to CTT and causing an amino acid substitution of Proline by Leucine. In At2g25970, the SNP was identified in exon-6 within the codon 1456th codon converting CAG, the codon for Glutamine into the stop codon UAG.

3.2 | Analysis of *ebss1* candidate genes by CRISPR/Cas9 mutagenesis

To identify the gene responsible for the *ebss1* mutant phenotype, we generated CRISPR/Cas9-induced mutant lines for At2g24610, At2g25220, and At2g25970 as described in Section 2. The CRISPR/Cas9 vector used in this study encoded sgRNAs that targeted exon-2 of At2g24610, exon-3 of At2g25220, and exon-1 of At2g25970, respectively (Figure 3a). As a result, various mutant alleles were detected, ranging from one or two base pair indels to a large deletion. Detailed information regarding the various types of mutation obtained and their effects are shown in Figure 3b.

Screening of CRISPR/Cas9-induced mutant lines of all three candidate genes for *ebss1* in the T3 generation revealed that the GFP fluorescence signals of the mutant lines At2g24610 and At2g25220 were similar to that of the reporter line, that is, they did not show the enhanced fluorescence phenotype typical for *ebss1*. In contrast, At2g25970 mutant plants exhibited a high GFP fluorescence phenotype (Figure 4a). To corroborate the finding, the first leaves from 50 T3 plants homozygous for mutant alleles of *At2g25970-1/2/3* each were harvested, and GFP fluorescence was quantified. Figure 4b shows that the GFP signal intensity of the CRISPR/Cas9 induced mutant lines (*At2g25970-1*, *At2g25970-2*, and *At2g25970-3*) is about 30% higher than the reporter line and similar to that of *ebss1*. We concluded from this finding that At2g25970, if mutated, leads to an increased GFP fluorescence and thus causes the *ebss1* phenotype.
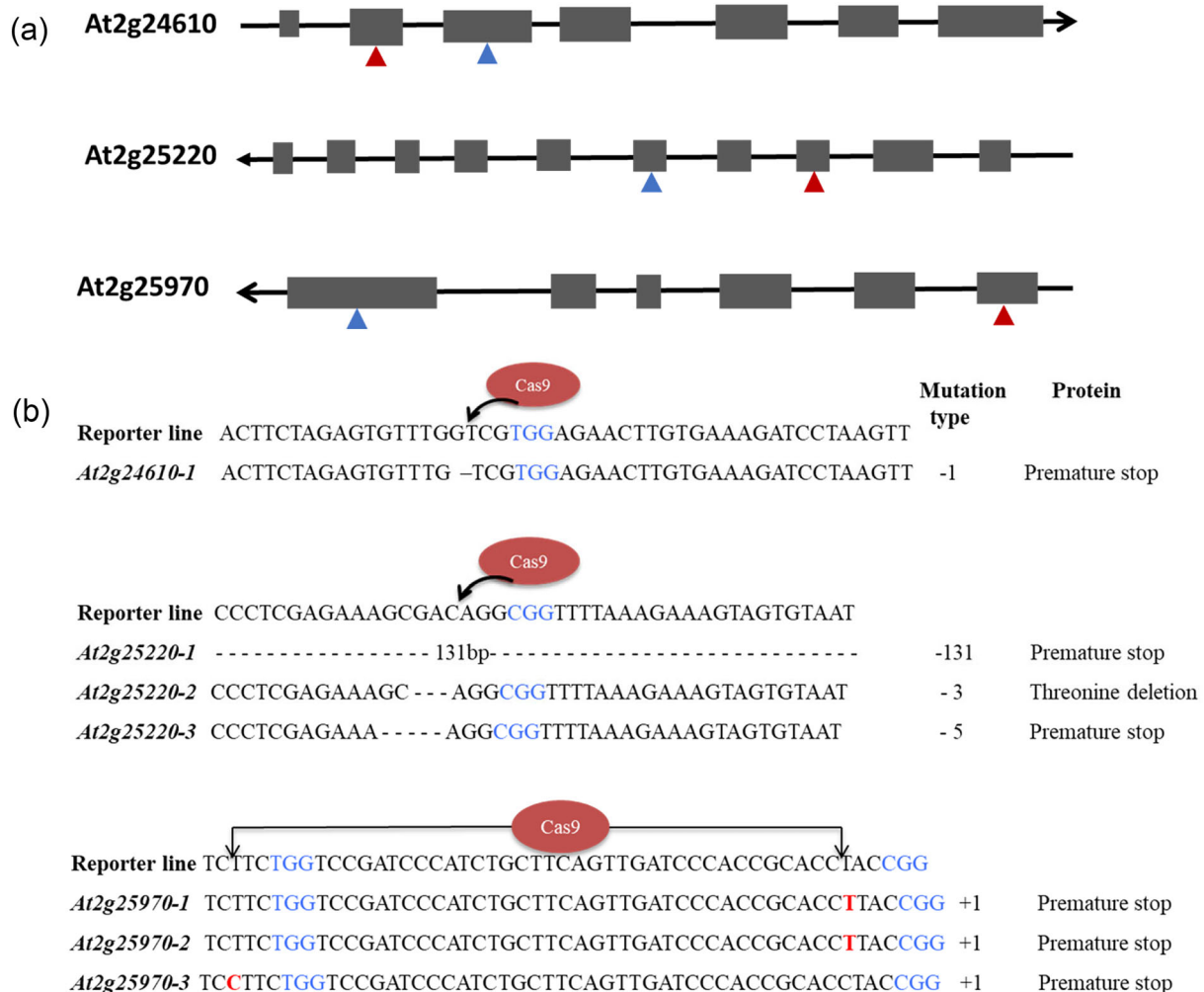

FIGURE 3 CRISPR/Cas9-induced mutations in *ebss1* candidate genes. (a) Location of the EMS (blue triangle) and the CRISPR/Cas9-induced mutations (red triangle) in At2g24610, At2g25220, and At2g25970. (b) CRISPR/Cas9-induced sequence changes and their effects on protein level in *ebss1* candidate genes. The Cas9 target regions are marked with arrows, and the PAM motif sequence is kept in light blue. Deletions are indicated by dashes and insertions by red letters.
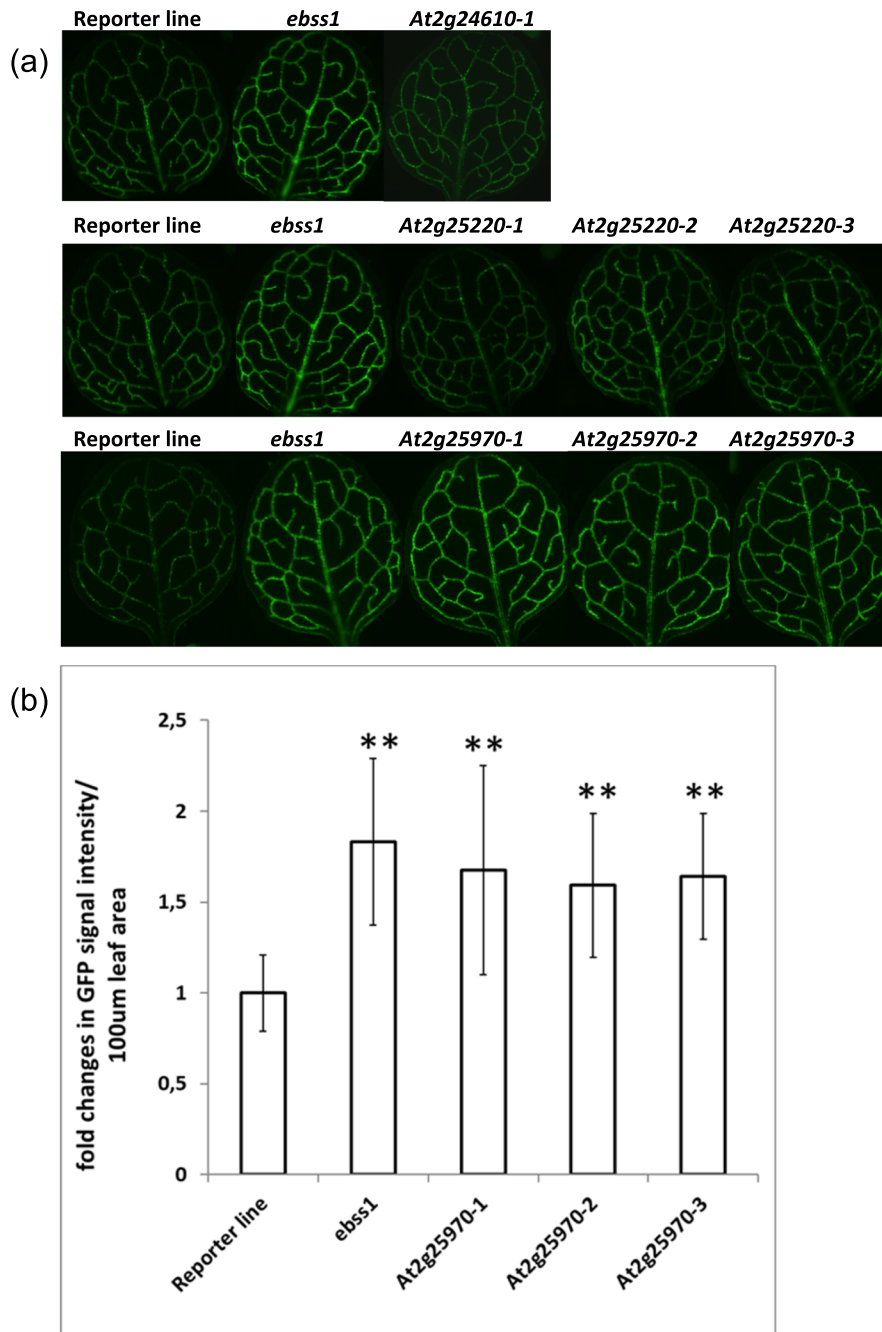
FIGURE 4 GFP fluorescent phenotype of CRISPR/Cas9-induced mutation in At2g24610, At2g25220, and At2g25970. (a) Leaf images of GFP fluorescence of the reporter line, *ebss1*, and Cas9-induced mutant lines of At2g24610, At2g25220, and At2g25970. (b) Quantification of GFP fluorescence of the reporter line, *ebss1*, and various mutant lines of At2g25970. The relative signal intensity was measured from the first leaves of 17-day-old plants, normalized with the leaf area, and compared with the reporter line. The data are shown as mean ± standard deviation from 50 plants with standard *t*-test ** indicating $P < .01$.

3.3 | At2g25970 encodes a K homology (KH) domain-containing protein

At2g25970 encodes an unknown protein that contains K homology (KH) domains. KH domains were first detected in the heterogeneous nuclear ribonucleoprotein K (hnRNP K) of metazoan (Siomi et al., 1993) and later in other organisms, among them plants (Lorkovic & Barta, 2002). KH domains function as nucleic acid recognition motifs and are found as single or multiple copies within a protein (Nicastro et al., 2015; Valverde et al., 2008). The At2g25970 protein contains two KH type 1 domains and is closely

related to At1g33680 and At4g10070 proteins of Arabidopsis (Figure S2).

3.4 | Phenotypic analysis of CRISPR/Cas9-induced *At2g25970* mutants

3.4.1 | At2g25970 transcript level

To determine whether mutations in At2g25970 affect transcript abundances of the gene, we performed quantitative RT-PCR analysis.
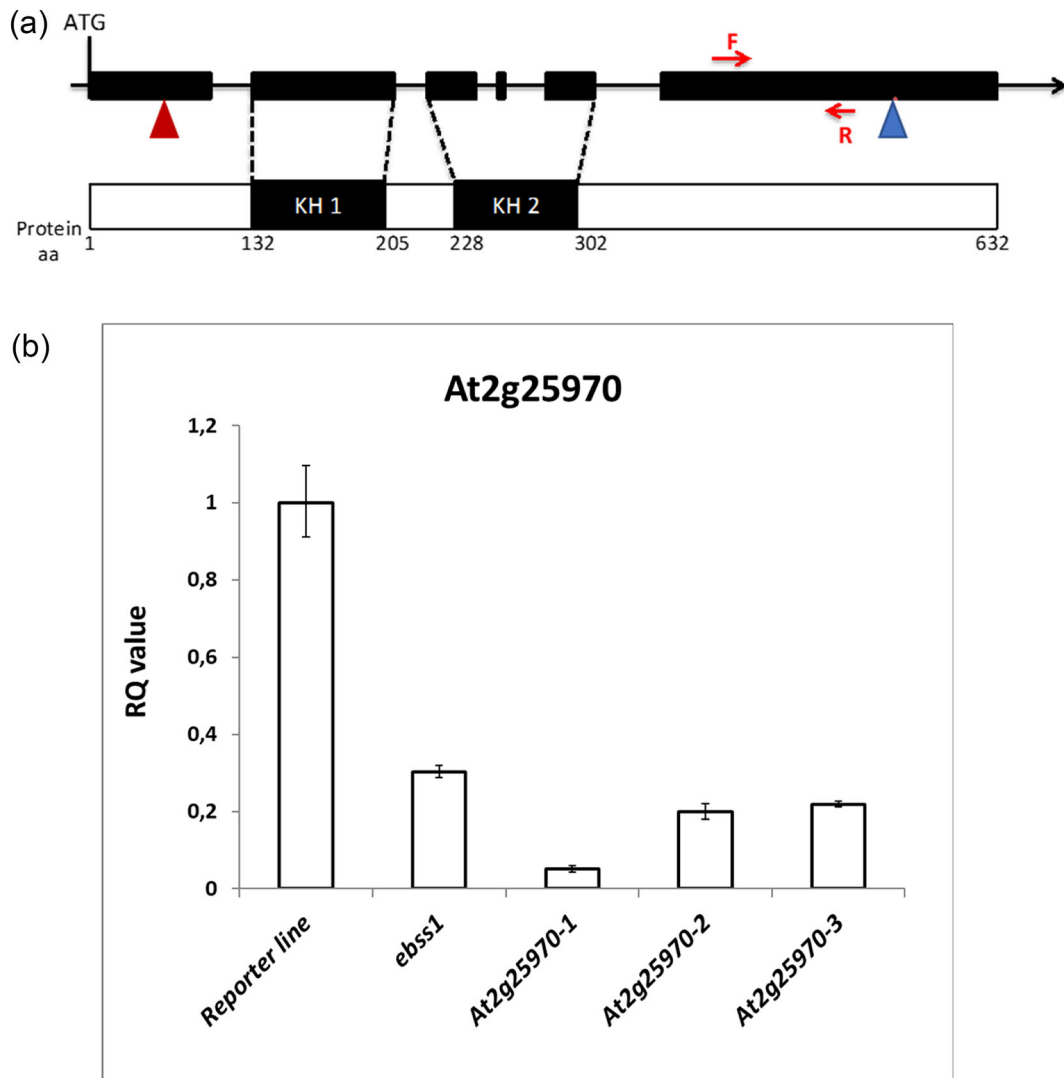
BANO and WESTHOFF

American Society
of Plant Biologists
Cultivating a better future through plant biology research

S E B SOCIETY FOR EXPERIMENTAL BIOLOGY

WILEY | 7 of 14

FIGURE 5 Transcript amounts of At2g25970 in EMS- and CRISPR/Cas9-induced *ebss1* mutant lines. (a) Schematic diagram of At2g25970 gene with EMS (blue triangle) and Cas9 target sites (red triangle) and the positions of forward (F) and reverse (R) primers (red arrows at exon-6) used to detect At2g25970 transcript level in reporter and mutant lines. Filled boxes represent exons. KH1 and KH2 in the diagram depict the K-homology domain region in the At2g25970 encoded protein (b) Transcript abundance of At2g25970 in reporter and mutant lines from 25-day-old seedlings. Three biological replicates were analyzed for each line. RQ (relative quantification) values show fold changes in transcript abundance as compared with the calibrator (reporter line). The error bar reflects variation among the biological replicates.

As shown in Figure 5, the expression of the At2g25970 gene is highly reduced in the CRISPR/Cas9-induced mutant lines (*At2g25970-1*, *At2g25970-2*, and *At2g25970-3*) as well as in the *ebss1* line compared with the reporter line.

3.4.2 | Growth characteristics

Major differences in plant growth and height were not observed for the mutant lines; however, in all mutants, the leaf areas were found to be increased as compared to the reporter line (Figures 6b/c). These differences in leaf areas were not observed in *ebss1* at an early stage of development (Figure 6a) but became prominent in later stages. Detailed examinations revealed that the increasing leaf area was due

to an increase in both the length and width of the leaf blade (Figure 6d).

The enlarged leaf area of the mutants *At2g25970-1/2/3* and *ebss1* as compared with the reporter line raised the question of whether this increase is due to cell enlargement, cell numbers, or a combination of both. To determine the contribution of cell division and expansion to the *At2g25970-1/2/3* mutants, transverse sections from leaf blades of the *At2g25970-1*, *ebss1*, and reporter line were analyzed by light microscopy. In both types of mutants, the vascular bundle was found to be expanded, and concomitantly, the number of bundle sheath cells had increased by two to three more cells (Figure 7). These findings suggest that the overall increase in the leaf area is caused by a general increase in the leaf cell numbers due to the expansion of the vascular bundle and the bundle sheath. Since the
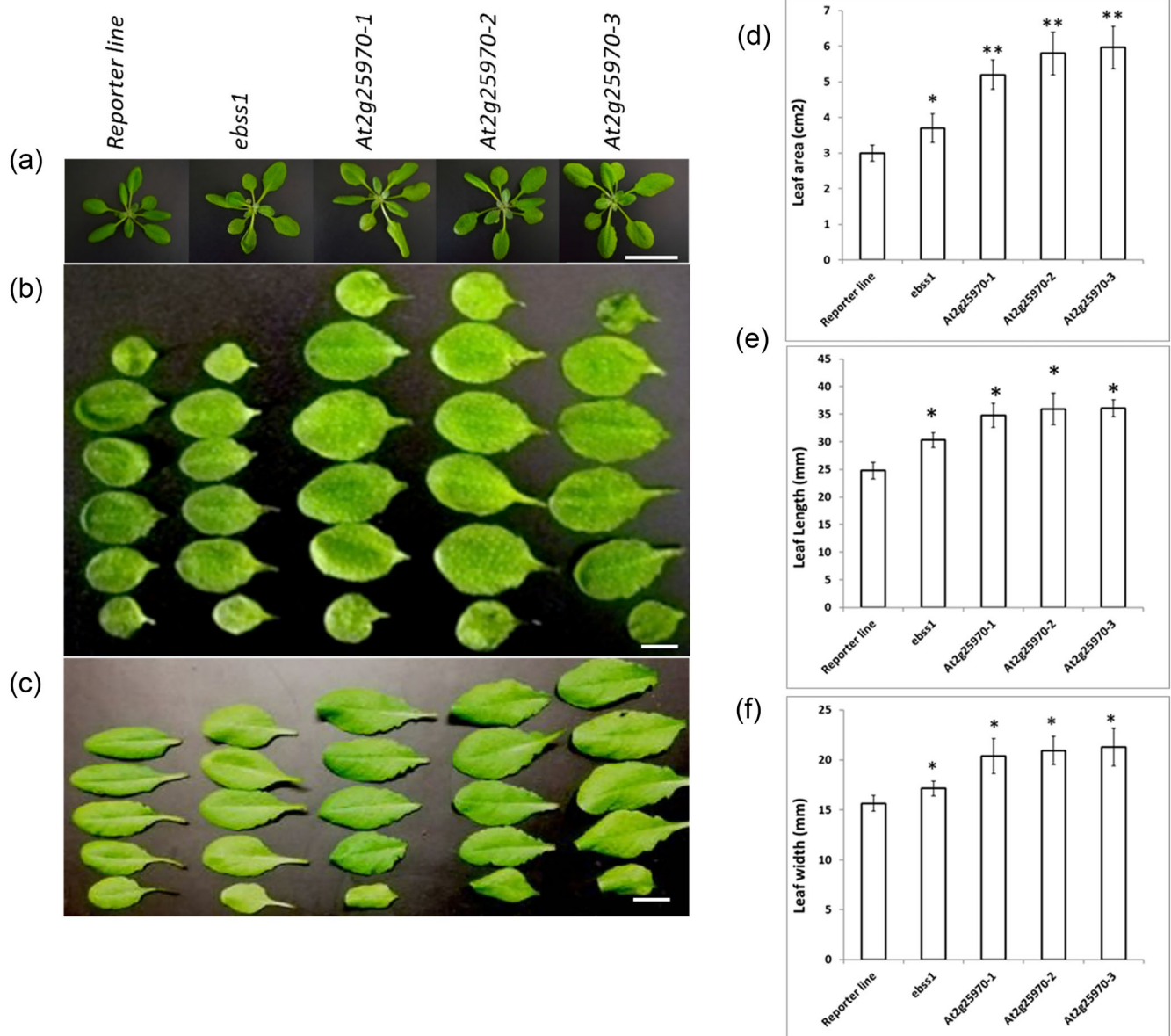
FIGURE 6 Leaf sizes of EMS- and CRISPR/Cas9-induced mutant lines at various ages. (a) Rosette phenotypes of 28-day-old EMS- and CRISPR/Cas9-induced mutant lines as compared with the reporter line. (b) Morphology of the first, second, and third rosette leaf of the reporter line, *ebss1*, and *At2g25970-1/2/3*. (c) Morphology of rosette leaves of 36-day-old plants. (d) Differences in leaf areas of 24-day-old reporter and mutant lines. The leaf area was measured from 10 individuals each. Data are shown as a mean ± standard deviation (SD) for each genotype; *t*-test: * $P < .05$; ** $P < .01$.

GLDPA promoter-driven GFP gene is active only in the bundle sheath and the vascular bundle (Engelmann et al., 2008). The finding also explains the enhanced GFP fluorescence as compared with the original reporter line.

3.4.3 | Trichome density

To investigate whether other leaf features have been altered in the At2g25970 mutant lines, we examined the leaf surface by fluorescent microscopy, and trichome numbers were counted in

At2g25970-1/2/3 and *ebss1* mutant plants as well as in plants of the reporter line (Figure 8a). The results obtained revealed a two-fold increase in trichome density in all At2g25970 mutants, including *ebss1* as compared with the reporter line (Figure 8b).

3.4.4 | Flowering time

Visual inspection of the growth behavior of *At2g25970-1/2/3* and *ebss1* mutant plants revealed a delay in flowering time (Figure 9). Bolting started 5–7 days earlier in the plants of the reporter line, and
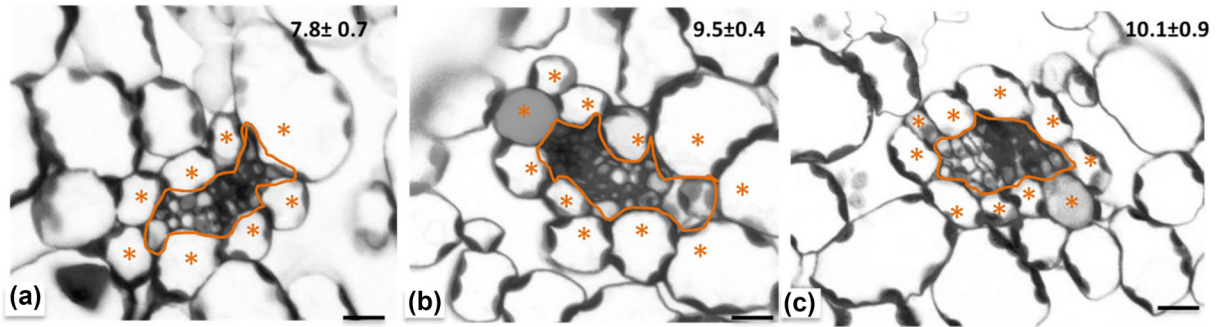
FIGURE 7 Anatomical analysis of bundle sheath cells in the third vein order of 25-day-old plants. Microscopic images of leaf cross sections of plants of the (a) reporter line, (b) ebss1, and (c) CRISPR/Cas9-induced mutant lines (At2g25970-1). Representative images are shown and the mean values of five individuals each are depicted in the upper right corner of the respective line. Scale bar: 10 µm.

FIGURE 8 Trichomes densities of *ebss1* and *At2g25970-1* mutant lines compared to the reporter line. (a) Representative images of the first leaves of 17-day-old reporter and mutant lines, *ebss1* and *At2g25970-1*. (b) Calculation of trichome densities from the first rosette leaf pair of reporter and mutant lines. Trichomes were counted from 20 individuals. ** indicates *t*-test $P < .01$.
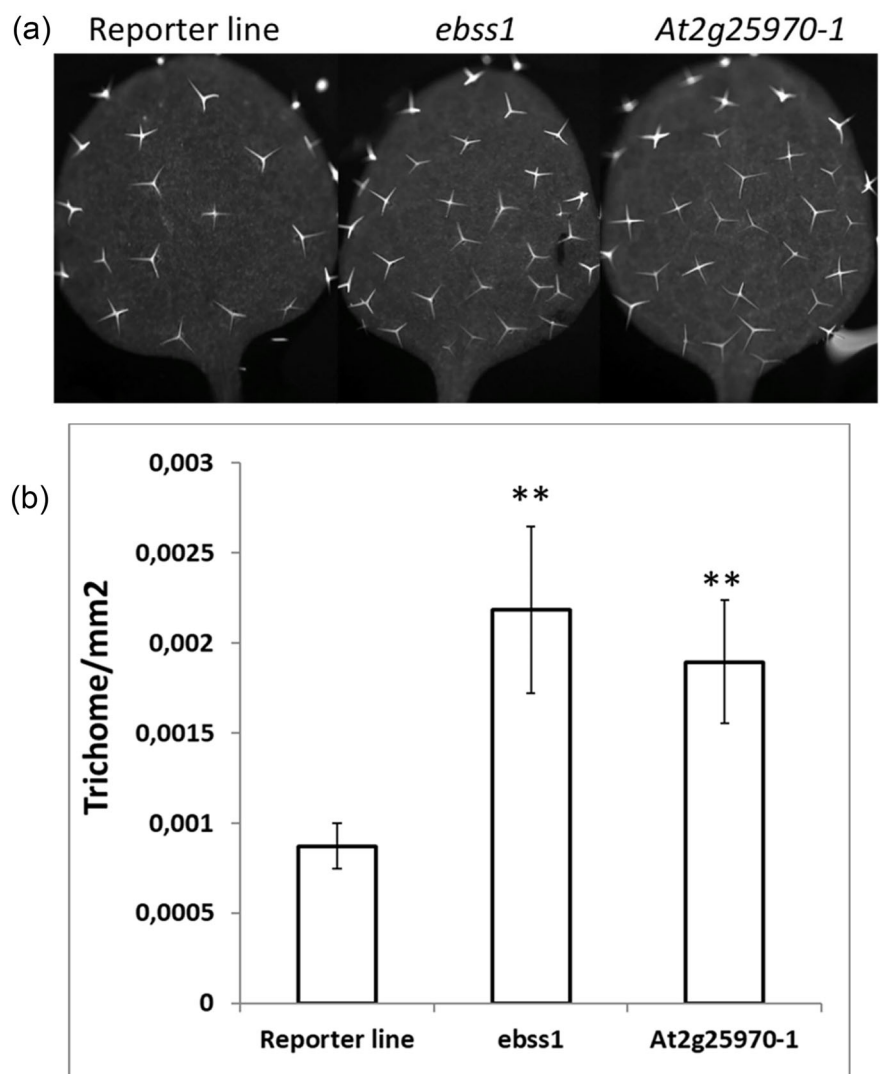
flowering of the mutant plants began about 7–8 days later (Figure 9). The finding suggests that defects in At2g25970 function extend the period of vegetative growth and thereby cause a delay in floral induction.

4 | DISCUSSION

We aimed at identifying genes for bundle sheath anatomy by pursuing a forward genetic approach using *A. thaliana* as a genetic model system

Genotype	Rosette leaves at bolting (n)	Time to bolting (d)	Time to Flowering (d)
Reporter line	13.5 ± 1.2	27.9 ± 1.2	30.9 ± 1.8
ebss1	13.6 ± 1.1	28.9 ± 1.5	32.5 ± 2.0[*]
At2g25970-1	16.4 ± 1.1	35.3 ± 2.7	38.2 ± 2.1[**]
At2g25970-2	15.0 ± 2.4	32.2 ± 3.3	35.8 ± 3.2[**]
At2g25970-3	15.4 ± 1.2	34.0 ± 2.6	37.9 ± 2.7[**]

FIGURE 9 Analysis of flowering time control in *ebss1* and Cas9-induced mutant lines (*At2g25970-1/2/3*) in comparison with the reporter line. (a) The flowering phenotypes of 36-day-old mutant lines (*ebss1*, *At2g25970-1/2/3*). (b) Quantification of flowering time parameters. For each line, 20 individual plants were analyzed. Data are shown as a mean ± standard deviation (SD) for each genotype; *t*-test: $*P < .05$; $** P < .01$.

and ethyl methanesulfonate as a mutagen. To easily recognize putative bundle sheath defective mutants, our genetic screen was based on a reporter line containing a chloroplast-targeted GFP gene that was driven by a bundle sheath preferential promoter. Using deviations in GFP fluorescence as a proxy for alteration in bundle sheath size or photosynthetic activity, we were able to identify numbers of stable mutants with an elevated or a faint GFP fluorescence phenotype, with many of them showing defects in bundle sheath anatomy (Döring et al., 2019). Pursuing a SHOREmap approach with nine selected mutants, we could map candidate genes in single genomic regions (Döring et al., 2019). For the study presented in this report, we have chosen the mutant lines *ebss1* to demonstrate that the mutant candidate genes identified by SNP calling in the mapping intervals can be successfully scrutinized by using CRISPR/Cas9 technology.

CRISPR/Cas9-mediated knock-outs of the candidate genes At2g24610, At2g25220, and At2g25970 revealed that At2g25970 was responsible for the enhanced GFP fluorescence phenotype shown by *ebss1*. At2g25970 encodes one of the 26 KH domain-containing proteins present in the *A. thaliana* genome (Lorkovic & Barta, 2002). The protein is 80%–90% conserved in Brassicacean species, and the sequence conservation to homologs from monocot species is mainly restricted to the KH domain (Figure S3). At2g25970 transcripts accumulate ubiquitously in both time and space (Klepikova et al., 2016; CATd.b http://urgv.evry.inra.fr/cgi-bin/projects/CATdb/catdb_projects_Ath.pl) suggesting a more general function of this gene and explaining the pleiotropic effects of its mutants.

Five of the KH domain proteins of *A. thaliana*, that is, HEN4 (Cheng et al., 2003), BTR1 (Fujisaki & Ishikawa, 2008), PEPPER (Ripoll et al., 2006), FLK (Lim et al., 2004), and RCF3 (Karlsson et al., 2015), have been functionally characterized, and all turned out to be multifunctional. Each of these proteins had multiple KH domains, which

may explain their multifunctionality. RCF3 (At5g53060), for example, has two PCBP-like KH domains, two KH-1 superfamily KH domains, and one KH type-1 KH domain and is involved in jasmonate signaling (Thatcher et al., 2015), miRNA biogenesis (Karlsson et al., 2015), pre-mRNA splicing (Cheng et al., 2003), and abiotic signaling processes (Jeong et al., 2013) (Figure S2).

The presence of multiple domains for RNA binding and protein–protein interactions (Gronland & Ramos, 2017; Mackereth & Sattler, 2012; Ottoz & Berchowitz, 2020) and the versatility of these proteins in recognizing both RNA and DNA (Debaize & Troadec, 2019; Hudson & Ortlund, 2014) make KH domain proteins ideal candidates for integrators of and in regulatory networks (Alvarez et al., 2021; Csizmok et al., 2016; Pawson & Nash, 2003). Similar to these five KH domain proteins, At2g25970 turned out to be multifunctional. In At2g25970 mutants, the *GLDPA* promoter-driven GFP reporter gene is more strongly expressed, the sizes of leaves and the density of trichomes increase, and the flowering date is delayed. The rise in leaf area and concomitantly in GFP fluorescence appears to be caused by an increased cell number in the bundle sheath and the vasculature suggesting that At2g25970 is involved in the regulation of cell division and/or the cell cycle.

In humans, the KH domain protein FUBP1 (Debaize & Troadec, 2019) has been shown to be involved in cell proliferation by activating c-Myc gene expression (Duncan et al., 1994). In plants, Myc-like, that is, basic helix–loop–helix (bHLH) proteins do not seem to play a major role in regulating cell division and/or cell cycle. In contrast, Myb proteins, their frequent interaction partners (Millard et al., 2019), are involved in cell cycle regulation (Vercruysse et al., 2020; Xie et al., 2010). Interestingly a Myc/Myb regulatory module has been shown to be involved in bundle sheath-specific gene expression in Arabidopsis (Dickinson et al., 2020).

Co-expression analyses of transcriptome data (https://www.michalopoulos.net/act/; https://atted.jp) support a possible role of At2g25970 in cell cycle regulation. Fluctuation in the expression of At2g25970 transcript has been observed during the G1 phase of the cell cycle (Menges et al., 2002). In addition, At2g25970 transcripts co-accumulate with CDKC;2 RNA levels. CDKC;2 is a cyclin-dependent protein kinase that phosphorylates the carboxyterminal domain of a large subunit of RNA polymerase II and is part of the so-called transcript elongation factor P-TEFb (Antosz et al., 2017). Zhao et al. (2017) found that the loss of *CDKC;2* function leads to an increase in lateral organ size because of a rise in cell division activity, indicating that *CDKC;2* acts as a negative regulator of cell division. A similar phenotype, that is, broader leaves and an increased number of bundle sheath and vascular cells, is also true for *At2g250970* mutant lines, suggesting that the At2g25970 protein is functionally associated with *CDKC;2* activity. Along these lines, *CDKC;2* transcript abundance was found to be substantially reduced in the *At2g25970* mutants as compared with the reporter line (Figure 10b).

CDKC;2 as the target of At2g25970 action may also explain the floral retardation observed for the mutant lines. Floral induction is a
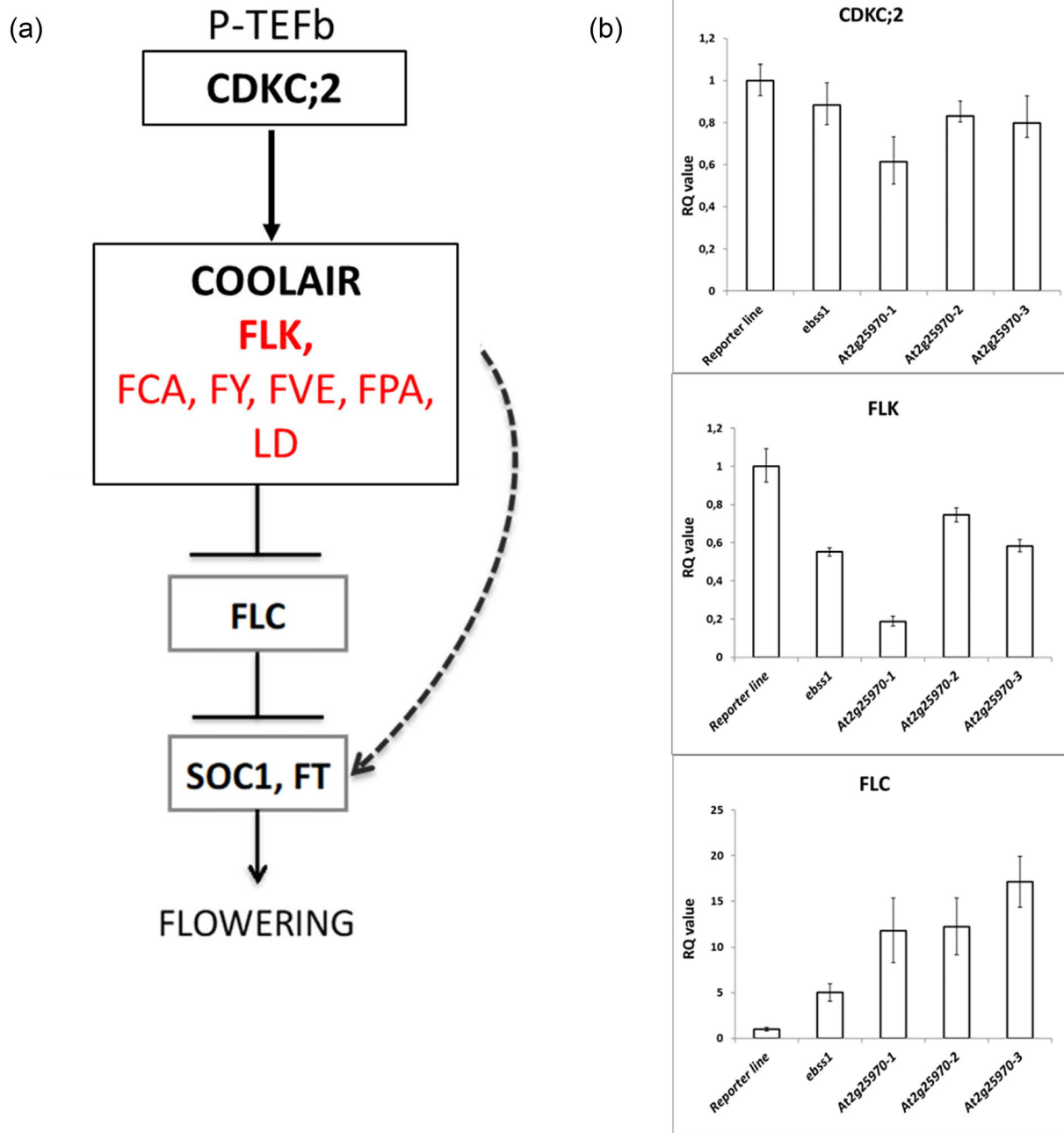

FIGURE 10 Impact of At2g25970 mutation on CDKC;2 transcript level and CDKC;2 regulated flowering time genes. (a) Schematic pathway of genes controlling flowering time in *A. thaliana* (modified from Henderson & Dean, 2004, and Wang et al., 2014). (b) Relative abundances of *CDKC;2*, *FLK*, and *FLC* transcripts in 25-day-old rosette leaves of the reporter line, *ebss1*, and the *At2g25970-1/2/3* mutant lines.

major developmental transition in plants and is regulated by various external and internal cues (Amasino, 2010). The floral repressor *FLOWERING LOCUS C* (*FLC*) plays a central role in floral induction and is the hub on which the autonomous and the vernalization pathways converge (Whittaker & Dean, 2017). The autonomous pathway is comprised of a variety of factors involved in RNA processing, among them the KH domain protein FLK and chromatin modification that together repress *FLC* activity. A long antisense RNA transcribed from the 3′ end into the *FLC* locus is processed, with the help of RNA processing components of the autonomous pathway, to various alternatively spliced and polyadenylated *FLC* antisense RNA, which are collectively called *COOLAIR* and that are involved in repressing *FLC* transcription by chromatin silencing (Wu et al., 2020). *COOLIAR* transcription is promoted by CDKC;2 activity (Wang et al., 2014), and the loss of *CDKC;2* functions, therefore, leads to a delay in flowering (Cui et al., 2007; Zhao et al., 2017) (Figure 10a). Quantification of transcript amounts from both *CDKC;2* and *FLK* revealed that both transcript levels were significantly reduced in *At2g25970* mutants (Figure 10b). In contrast, but as expected, *FLC* transcript abundance was higher in the mutants as compared with the reporter line (Figure 10b).

Taken together, the available evidence suggests that the mutant phenotypes in flowering time are brought about via *CDKC;2*, which in turn is functionally connected to *At2g25970* activity. It is completely unclear at present, how this functional connection could be achieved mechanistically. Quite recently, another KH domain protein encoded by *FLOWERING LOCUS Y* (At1g33680) has been reported to delay flowering when mutated (Dai et al., 2020) suggesting redundancy and overlapping functions in this family of RNA-binding proteins.

We have pursued a forward genetic screen with a reporter line of Arabidopsis to identify mutants affected in bundle sheath anatomy. We have achieved to locate candidate genes by a mapping by sequencing strategy (Döring et al., 2019). By using CRISPR/Cas9 technology, we have been able to identify the causative gene among the various candidate genes located in the mapping interval. Our experimental strategy may thus be considered successful, since At2g25970, when mutated, indeed leads to an inflated bundle sheath. However, the gene acts pleiotropically and affects also other developmental or physiological processes such as trichome density and flowering time. The pleiotropic behavior of At2g25970 function may be explained by its nature, since At2g25970 encodes a KH domain protein that could interact with *CDKC;2*, a component of a transcription elongation factor complex of RNA polymerase II (Antosz et al., 2017). It remains to be seen, therefore, whether further exploitation of the remaining mutant library will lead to the identification of novel and specific regulators of bundle sheath anatomy, which would be highly desirable for C_4 engineering.

AUTHOR CONTRIBUTIONS

Peter Westhoff developed the overall study design. Zahida Bano carried out all experiments and analyzed the data. Peter Westhoff and Zahida Bano wrote the manuscript together.

CONFLICT OF INTEREST STATEMENT

The authors did not report any conflict of interest.

PEER REVIEW

The peer review history for this article is available in the Supporting Information for this article.

DATA AVAILABILITY STATEMENT

All study data are included in the main text and supporting information.

ORCID

Zahida Bano https://orcid.org/0009-0008-3341-4804
Peter Westhoff https://orcid.org/0000-0002-4621-1490

REFERENCES

Akhani, H., & Khoshravesh, R. (2013). The relationship and different C4 Kranz anatomy of Bassia eriantha and Bassia eriophora, two often confused Irano-Turanian and Saharo-Sindian species. *Phytotaxa*, *93*, 1–24. https://doi.org/10.11646/phytotaxa.93.1.1

Alvarez, J. M., Brooks, M. D., Swift, J., & Coruzzi, G. M. (2021). Time-based systems biology approaches to capture and model dynamic gene regulatory networks. *Annual Review of Plant Biology*, *72*, 105–131. https://doi.org/10.1146/annurev-arplant-081320-090914

Amasino, R. (2010). Seasonal and developmental timing of flowering. *The Plant Journal*, *61*, 1001–1013.

Antosz, W., Pfab, A., Ehrnsberger, H. F., Holzinger, P., Kollen, K., Mortensen, S. A., Bruckmann, A., Schubert, T., Langst, G., Griesenbeck, J., Schubert, V., Grasser, M., & Grasser, K. D. (2017). The composition of the Arabidopsis RNA polymerase II transcript elongation complex reveals the interplay between elongation and mRNA processing factors. *Plant Cell*, *29*, 854–870. https://doi.org/10.1105/tpc.16.00735

Cheng, Y. L., Kato, N., Wang, W. M., Li, J. J., & Chen, X. M. (2003). Two RNA binding proteins, HEN4 and HUM, act in the processing of AGAMOUS pre-mRNA in Arabidopsis thaliana. *Developmental Cell*, *4*, 53–66. https://doi.org/10.1016/S1534-5807(02)00399-4

Conklin, P. A., Strable, J., Li, S., & Scanlon, M. J. (2019). On the mechanisms of development in monocot and eudicot leaves. *The New Phytologist*, *221*, 706–724. https://doi.org/10.1111/nph.15371

Csizmok, V., Follis, A. V., Kriwacki, R. W., & Forman-Kay, J. D. (2016). Dynamic protein interaction networks and new structural paradigms in signaling. *Chemical Reviews*, *116*, 6424–6462. https://doi.org/10.1021/acs.chemrev.5b00548

Cui, X., Fan, B., Scholz, J., & Chen, Z. (2007). Roles of Arabidopsis cyclin-dependent kinase C complexes in cauliflower mosaic virus infection,

plant growth, and development. *Plant Cell*, *19*, 1388–1402. https://doi.org/10.1105/tpc.107.051375

Dai, G. Y., Chen, D. K., Sun, Y. P., Liang, W. Y., Liu, Y., Huang, L. Q., Li, Y. K., He, J. F., & Yao, N. (2020). The Arabidopsis KH-domain protein FLOWERING LOCUS Y delays flowering by upregulating FLOWERING LOCUS C family members. *Plant Cell Reports*, *39*, 1705–1717. https://doi.org/10.1007/s00299-020-02598-w

Debaize, L., & Troadec, M. B. (2019). The master regulator FUBP1: Its emerging role in normal cell function and malignant development. *Cellular and Molecular Life Sciences*, *76*, 259–281. https://doi.org/10.1007/s00018-018-2933-6

Dengler, N. G., & Nelson, T. (1999). Leaf structure and development in C4 plants. In R. F. Sage & R. K. Monson (Eds.), *C4 plant biology* (pp. 133–172). Academic Press.

Dickinson, P. J., Knerova, J., Szecowka, M., Stevenson, S. R., Burgess, S. J., Mulvey, H., Bagman, A. M., Gaudinier, A., Brady, S. M., & Hibberd, J. M. (2020). A bipartite transcription factor module controlling expression in the bundle sheath of Arabidopsis thaliana. *Nature Plants*, *6*, 1468–1479. https://doi.org/10.1038/s41477-020-00805-w

Döring, F., Billakurthi, K., Gowik, U., Sultmanis, S., Khoshravesh, R., Das Gupta, S., Sage, T. L., & Westhoff, P. (2019). Reporter-based forward genetic screen to identify bundle sheath anatomy mutants in A. thaliana. *The Plant Journal*, *97*, 984–995. https://doi.org/10.1111/tpj.14165

Duncan, R., Bazar, L., Michelotti, G., Tomonaga, T., Krutzsch, H., Avigan, M., & Levens, D. (1994). A sequence-specific, single-strand binding protein activates the far upstream element of c-myc and defines a new DNA-binding motif. *Genes & Development*, *8*, 465–480. https://doi.org/10.1101/gad.8.4.465

Emmerling, J. (2018). Studies into the regulation of C4 photosynthesis—Towards factors controlling bundle sheath expression and Kranz anatomy development. In *Mathematisch-Naturwissenschaftliche Fakultät*. Heinrich-Heine-Universität Düsseldorf.

Engelmann, S., Wiludda, C., Burscheidt, J., Gowik, U., Schlue, U., Koczor, M., Streubel, M., Cossu, R., Bauwe, H., & Westhoff, P. (2008). The gene for the P-subunit of glycine decarboxylase from the C4 species *Flaveria trinervia*: Analysis of transcriptional control in transgenic *Flaveria bidentis* (C4) and *Arabidopsis thaliana* (C3). *Plant Physiology*, *146*, 1773–1785. https://doi.org/10.1104/pp.107.114462

Ermakova, M., Danila, F. R., Furbank, R. T., & von Caemmerer, S. (2020). On the road to C4 rice: Advances and perspectives. *The Plant Journal*, *101*, 940–950. https://doi.org/10.1111/tpj.14562

Fujisaki, K., & Ishikawa, M. (2008). Identification of an Arabidopsis thaliana protein that binds to tomato mosaic virus genomic RNA and inhibits its multiplication. *Virology*, *380*, 402–411. https://doi.org/10.1016/j.virol.2008.07.033

Gibson, D. G., Young, L., Chuang, R. Y., Venter, J. C., Hutchison, C. A., & Smith, H. O. (2009). Enzymatic assembly of DNA molecules up to several hundred kilobases. *Nature Methods*, *6*, 343–345. https://doi.org/10.1038/nmeth.1318

Gronland, G. R., & Ramos, A. (2017). The devil is in the domain: Understanding protein recognition of multiple RNA targets. *Biochemical Society Transactions*, *45*, 1305–1311. https://doi.org/10.1042/BST20160362

Hahn, F., Eisenhut, M., Mantegazza, O., & Weber, A. P. M. (2017). Generation of targeted knockout mutants in Arabidopsis thaliana using CRISPR/Cas9. *Bio-Protocol*, *7*, e2384. https://doi.org/10.21769/BioProtoc.2384

Hatch, M. D. (1987). C$_4$ photosynthesis: A unique blend of modified biochemistry, anatomy and ultrastructure. *Biochimica et Biophysica Acta*, *895*, 81–106. https://doi.org/10.1016/S0304-4173(87)80009-5

Henderson, I. R., & Dean, C. (2004). Control of Arabidopsis flowering: The chill before the bloom. *Development*, *131*, 3829–3838. https://doi.org/10.1242/dev.01294

Hudson, W. H., & Ortlund, E. A. (2014). The structure, function and evolution of proteins that bind DNA and RNA. *Nature Reviews. Molecular Cell Biology*, *15*, 749–760. https://doi.org/10.1038/nrm3884

Jeong, I. S., Fukudome, A., Aksoy, E., Bang, W. Y., Kim, S., Guan, Q., Bahk, J. D., May, K. A., Russell, W. K., Zhu, J., & Koiwa, H. (2013). Regulation of abiotic stress signalling by Arabidopsis C-terminal domain phosphatase-like 1 requires interaction with a k-homology domain-containing protein. *PLoS ONE*, *8*, e80509. https://doi.org/10.1371/journal.pone.0080509

Karlsson, P., Christie, M. D., Seymour, D. K., Wang, H., Wang, X., Hagmann, J., Kulcheski, F., & Manavella, P. A. (2015). KH domain protein RCF3 is a tissue-biased regulator of the plant miRNA biogenesis cofactor HYL1. *Proceedings of the National Academy of Sciences of the United States of America*, *112*, 14096–14101. https://doi.org/10.1073/pnas.1512865112

Kirschner, S., Woodfield, H., Prusko, K., Koczor, M., Gowik, U., Hibberd, J. M., & Westhoff, P. (2018). Expression of SULTR2;2, encoding a low-affinity sulphur transporter, in the Arabidopsis bundle sheath and vein cells is mediated by a positive regulator. *Journal of Experimental Botany*, *69*, 4897–4906. https://doi.org/10.1093/jxb/ery263

Klepikova, A. V., Kasianov, A. S., Gerasimov, E. S., Logacheva, M. D., & Penin, A. A. (2016). A high resolution map of the Arabidopsis thaliana developmental transcriptome based on RNA-seq profiling. *The Plant Journal*, *88*, 1058–1070. https://doi.org/10.1111/tpj.13312

Lazo, G. R., Stein, P. A., & Ludwig, R. A. (1991). A DNA transformation-competent *Arabidopsis* genomic library in *Agrobacterium*. *Biotechnology*, *9*, 963–967. https://doi.org/10.1038/nbt1091-963

Lim, M. H., Kim, J., Kim, Y. S., Chung, K. S., Seo, Y. H., Lee, I., Hong, C. B., Kim, H. J., & Park, C. M. (2004). A new Arabidopsis gene, FLK, encodes an RNA binding protein with K homology motifs and regulates flowering time via FLOWERING LOCUS C. *Plant Cell*, *16*, 731–740. https://doi.org/10.1105/tpc.019331

Long, S. P., Marshall-Colon, A., & Zhu, X. G. (2015). Meeting the global food demand of the future by engineering crop photosynthesis and yield potential. *Cell*, *161*, 56–66. https://doi.org/10.1016/j.cell.2015.03.019

Lorkovic, Z., & Barta, A. (2002). Genome analysis: RNA recognition motif (RRM) and K homology (KH) domain RNA-binding proteins from the flowering plant Arabidopsis thaliana. *Nucleic Acids Research*, *30*, 623–635. https://doi.org/10.1093/nar/30.3.623

Mackereth, C. D., & Sattler, M. (2012). Dynamics in multi-domain protein recognition of RNA. *Current Opinion in Structural Biology*, *22*, 287–296. https://doi.org/10.1016/j.sbi.2012.03.013

Menges, M., Hennig, L., Gruissem, W., & Murray, J. A. (2002). Cell cycle-regulated gene expression in Arabidopsis. *The Journal of Biological Chemistry*, *277*, 41987–42002. https://doi.org/10.1074/jbc.M207570200

Millard, P. S., Weber, K., Kragelund, B. B., & Burow, M. (2019). Specificity of MYB interactions relies on motifs in ordered and disordered contexts. *Nucleic Acids Research*, *47*, 9592–9608. https://doi.org/10.1093/nar/gkz691

Mitchell, P. L., & Sheehy, J. E. (2006). Supercharging rice photosynthesis to increase yield. *The New Phytologist*, *171*, 688–693. https://doi.org/10.1111/j.1469-8137.2006.01855.x

Nakayama, H., Leichty, A. R., & Sinha, N. R. (2022). Molecular mechanisms underlying leaf development, morphological diversification, and beyond. *Plant Cell*, *34*, 2534–2548. https://doi.org/10.1093/plcell/koac118

Nelissen, H., Gonzalez, N., & Inze, D. (2016). Leaf growth in dicots and monocots: So different yet so alike. *Current Opinion in Plant Biology*, *33*, 72–76. https://doi.org/10.1016/j.pbi.2016.06.009

Nicastro, G., Taylor, I. A., & Ramos, A. (2015). KH-RNA interactions: Back in the groove. *Current Opinion in Structural Biology*, *30*, 63–70. https://doi.org/10.1016/j.sbi.2015.01.002

Nikolov, L. A., Runions, A., Das Gupta, M., & Tsiantis, M. (2019). Leaf development and evolution. *Current Topics in Developmental Biology*, *131*, 109–139. https://doi.org/10.1016/bs.ctdb.2018.11.006

Ort, D. R., Merchant, S. S., Alric, J., Barkan, A., Blankenship, R. E., Bock, R., Croce, R., Hanson, M. R., Hibberd, J. M., Long, S. P., Moore, T. A., Moroney, J., Niyogi, K. K., Parry, M. A., Peralta-Yahya, P. P., Prince, R. C., Redding, K. E., Spalding, M. H., van Wijk, K. J., … Zhu, X. G. (2015). Redesigning photosynthesis to sustainably meet global food and bioenergy demand. *Proceedings of the National Academy of Sciences of the United States of America*, *112*, 8529–8536. https://doi.org/10.1073/pnas.1424031112

Ottoz, D. S. M., & Berchowitz, L. E. (2020). The role of disorder in RNA binding affinity and specificity. *Open Biology*, *10*, 200328. https://doi.org/10.1098/rsob.200328

Page, D. R., & Grossniklaus, L. (2002). The art and design of genetic screens: Arabidopsis thaliana. *Nature Reviews. Genetics*, *3*, 124–136. https://doi.org/10.1038/nrg730

Pawson, T., & Nash, P. (2003). Assembly of cell regulatory systems through protein interaction domains. *Science*, *300*, 445–452. https://doi.org/10.1126/science.1083653

Ripoll, J. J., Ferrándiz, C., Martínez-Laborda, A., & Vera, A. (2006). PEPPER, a novel K-homology domain gene, regulates vegetative and gynoecium development in Arabidopsis. *Developmental Biology*, *289*, 346–359. https://doi.org/10.1016/j.ydbio.2005.10.037

Schiml, S., Fauser, F., & Puchta, H. (2014). The CRISPR/Cas system can be used as nuclease for in planta gene targeting and as paired nickases for directed mutagenesis in Arabidopsis resulting in heritable progeny. *The Plant Journal*, *80*, 1139–1150. https://doi.org/10.1111/tpj.12704

Schneeberger, K., Ossowski, S., Lanz, C., Juul, T., Petersen, A. H., Nielsen, K. L., Jorgensen, J. E., Weigel, D., & Andersen, S. U. (2009). SHOREmap: Simultaneous mapping and mutation identification by deep sequencing. *Nature Methods*, *6*, 550–551. https://doi.org/10.1038/nmeth0809-550

Schneider, C. A., Rasband, W. S., & Eliceiri, K. W. (2012). NIH image to ImageJ: 25 years of image analysis. *Nature Methods*, *9*, 671–675. https://doi.org/10.1038/nmeth.2089

Sedelnikova, O. V., Hughes, T. E., & Langdale, J. A. (2018). Understanding the genetic basis of C4 Kranz anatomy with a view to engineering C3 crops. *Annual Review of Genetics*, *52*, 249–270. https://doi.org/10.1146/annurev-genet-120417-031217

Siomi, H., Matunis, M. J., Michael, W. M., & Dreyfuss, G. (1993). The pre-mRNA binding K protein contains a novel evolutionary conserved motif. *Nucleic Acids Research*, *21*, 1193–1198. https://doi.org/10.1093/nar/21.5.1193

Thatcher, L. F., Kamphuis, L. G., Hane, J. K., Oñate-Sánchez, L., & Singh, K. B. (2015). The Arabidopsis KH-domain RNA-binding protein ESR1 functions in components of jasmonate signaling, unlinking growth restraint and resistance to stress. *PLoS ONE*, *10*, e0126978. https://doi.org/10.1371/journal.pone.0126978

Valverde, R., Edwards, L., & Regan, L. (2008). Structure and function of KH domains. *The FEBS Journal*, *275*, 2712–2726. https://doi.org/10.1111/j.1742-4658.2008.06411.x

Vercruysse, J., Baekelandt, A., Gonzalez, N., & Inze, D. (2020). Molecular networks regulating cell division during Arabidopsis leaf growth. *Journal of Experimental Botany*, *71*, 2365–2378. https://doi.org/10.1093/jxb/erz522

Wang, Z. W., Wu, Z., Raitskin, O., Sun, Q., & Dean, C. (2014). Antisense-mediated FLC transcriptional repression requires the P-TEFb transcription elongation factor. *Proceedings of the National Academy of Sciences of the United States of America*, *111*, 7468–7473. https://doi.org/10.1073/pnas.1406635111

Westhoff, P., & Gowik, U. (2010). Evolution of C4 photosynthesis—Looking for the master switch. *Plant Physiology*, *154*, 598–601. https://doi.org/10.1104/pp.110.161729

Whittaker, C., & Dean, C. (2017). The FLC locus: A platform for discoveries in epigenetics and adaptation. *Annual Review of Cell and Developmental Biology*, *33*, 555–575.

Wiludda, C., Schulze, S., Gowik, U., Engelmann, S., Koczor, M., Streubel, M., Bauwe, H., & Westhoff, P. (2012). Regulation of the photorespiratory *GLDPA* gene in C4 *Flaveria*—An intricate interplay of transcriptional and post-transcriptional processes. *Plant Cell*, *24*, 137–151. https://doi.org/10.1105/tpc.111.093872

Wu, Z., Fang, X., Zhu, D., & Dean, C. (2020). Autonomous pathway: FLOWERING LOCUS C repression through an antisense-mediated chromatin-silencing mechanism. *Plant Physiology*, *182*, 27–37. https://doi.org/10.1104/pp.19.01009

Xie, Z., Lee, E., Lucas, J. R., Morohashi, K., Li, D., Murray, J. A., Sack, F. D., & Grotewold, E. (2010). Regulation of cell proliferation in the stomatal lineage by the Arabidopsis MYB FOUR LIPS via direct targeting of core cell cycle genes. *Plant Cell*, *22*, 2306–2321. https://doi.org/10.1105/tpc.110.074609

Zhang, X., Henriques, R., Lin, S. S., Niu, Q. W., & Chua, N. H. (2006). Agrobacterium-mediated transformation of Arabidopsis thaliana using the floral dip method. *Nature Protocols*, *1*, 641–646. https://doi.org/10.1038/nprot.2006.97

Zhao, L., Li, Y., Xie, Q., & Wu, Y. (2017). Loss of CDKC;2 increases both cell division and drought tolerance in Arabidopsis thaliana. *The Plant Journal*, *91*, 816–828. https://doi.org/10.1111/tpj.13609

SUPPORTING INFORMATION

Additional supporting information can be found online in the Supporting Information section at the end of this article.